

Harvard University
Harvard University Biostatistics Working Paper Series

Year 2005

Paper 32

Computational Techniques for Spatial Logistic
Regression with Large Datasets

Christopher J. Paciorek*

Louise Ryan†

*Harvard School of Public Health, paciorek@hsph.harvard.edu

†Harvard School of Public Health and Dana-Farber Cancer Institute, lryan@hsph.harvard.edu

This working paper is hosted by The Berkeley Electronic Press (bepress) and may not be commercially reproduced without the permission of the copyright holder.

<http://biostats.bepress.com/harvardbiostat/paper32>

Copyright ©2005 by the authors.

Computational Techniques for Spatial Logistic Regression with Large Datasets

Christopher J. Paciorek and Louise Ryan

Abstract

In epidemiological work, outcomes are frequently non-normal, sample sizes may be large, and effects are often small. To relate health outcomes to geographic risk factors, fast and powerful methods for fitting spatial models, particularly for non-normal data, are required. We focus on binary outcomes, with the risk surface a smooth function of space. We compare penalized likelihood models, including the penalized quasi-likelihood (PQL) approach, and Bayesian models based on fit, speed, and ease of implementation.

A Bayesian model using a spectral basis representation of the spatial surface provides the best tradeoff of sensitivity and specificity in simulations, detecting real spatial features while limiting overfitting and being more efficient computationally than other Bayesian approaches. One of the contributions of this work is further development of this underused representation. The spectral basis model outperforms the penalized likelihood methods, which are prone to overfitting, but is slower to fit and not as easily implemented. Conclusions based on a real dataset of cancer cases in Taiwan are similar albeit less conclusive with respect to comparing the approaches.

The success of the spectral basis with binary data and similar results with count data suggest that it may be generally useful in spatial models and more complicated hierarchical models.

Computational techniques for spatial logistic regression with large datasets

Christopher J. Paciorek and Louise Ryan *

6th October 2005

key words: Bayesian statistics, Fourier basis, FFT, generalized linear mixed model, geostatistics, spatial statistics, spectral basis

1 Abstract

In epidemiological work, outcomes are frequently non-normal, sample sizes may be large, and effects are often small. To relate health outcomes to geographic risk factors, fast and powerful methods for fitting spatial models, particularly for non-normal data, are required. We focus on binary outcomes, with the risk surface a smooth function of space. We compare penalized likelihood models, including the penalized quasi-likelihood (PQL) approach, and Bayesian models based on fit, speed, and ease of implementation.

A Bayesian model using a spectral basis representation of the spatial surface provides the best tradeoff of sensitivity and specificity in simulations, detecting real spatial features while limiting overfitting and being more efficient computationally than other Bayesian approaches. One of the contributions of this work is further development of this underused representation. The spectral basis model outperforms the penalized likelihood methods, which are prone to overfitting, but is slower to fit and not as easily implemented. Conclusions based on a real dataset of cancer cases in Taiwan are similar albeit less conclusive with respect to comparing the approaches.

The success of the spectral basis with binary data and similar results with count data suggest that it may be generally useful in spatial models and more complicated hierarchical models.

*Christopher Paciorek is Assistant Professor, Department of Biostatistics, Harvard School of Public Health, 655 Huntington Avenue, Boston, MA 02115 (E-mail: paciorek@alumni.cmu.edu). Louise Ryan is Professor, Department of Biostatistics, Harvard School of Public Health, 655 Huntington Avenue, Boston, MA 02115 (E-mail: lryan@hsph.harvard.edu)

2 Introduction

Epidemiological investigations that assess how health outcomes are related to risk factors that vary geographically are becoming increasingly popular. This paper is motivated by an ongoing epidemiological study in Kaohsiung, Taiwan, a center of petrochemical production, for which administrative data suggest excess cancer deaths amongst residents less than 20 years old living within 3 km of a plant (Pan et al. 1994). A full case-control study is in progress to investigate this suspected link between plant emissions and cancer, with the residences of individuals being geocoded to allow for spatial modelling. Such individual-level or point-referenced data are becoming increasingly common in epidemiology with the use of geographic information systems (GIS) and geocoding of addresses. In contrast to health data aggregated into regions, often fit using Markov random field models (Waller, Carlin, Xia, and Gelfand 1997; Best, Arnold, Thomas, Waller, and Conlon 1999; Banerjee, Carlin, and Gelfand 2004), analysis of individual-level data (often called geostatistics) avoids both ecological bias (Greenland 1992; Richardson 1992; Best, Ickstadt, and Wolpert 2000) and reliance on arbitrary regional boundaries, but introduces computational difficulties.

In this paper, we focus on methods for fitting models for Bernoulli response data with the outcome a binary variable indicating disease or health status. The specific model we investigate is a logistic regression,

$$\begin{aligned} Y_i &\sim \text{Ber}(p(\mathbf{x}_i, \mathbf{s}_i)) \\ \text{logit}(p(\mathbf{x}_i, \mathbf{s}_i)) &= \mathbf{x}_i^T \boldsymbol{\beta} + g_{\boldsymbol{\theta}}(\mathbf{s}_i), \end{aligned} \quad (1)$$

where Y_i , $i = 1, \dots, n$, is the binary status of the i th subject; $g_{\boldsymbol{\theta}}(\cdot)$ is a smooth function, parameterized by $\boldsymbol{\theta}$, of the spatial location of subject i , $\mathbf{s}_i \in \mathbb{R}^2$; and \mathbf{x}_i is a vector of additional individual-level covariates of interest. One application of this model is to the analysis of case-control data. For binary outcomes with the logit link, the use of a retrospective case-control design in place of random sampling from the population increases the power for assessing relative risk based on the covariates, including any spatial effect, but prevents one from estimating the absolute risk of being a case (Carroll, Ruppert, and Stefanski 1995, p. 182; Elliott, Wakefield, Best, and Briggs 2000).

There have been two basic approaches to modelling the spatial function, $g_{\boldsymbol{\theta}}(\cdot)$, each with a variety of parameterizations. One approach treats it as spatially correlated random effects, in which case (1) is a generalized linear mixed model (GLMM) (McCulloch and Searle 2001; Ruppert, Wand, and Carroll 2003). A second approach considers the spatial function to be a regression term, in this case a two-dimensional smooth term, in which case (1) is a standard generalized additive model (GAM) (Hastie and Tibshirani 1990; Diggle, Tawn, and Moyeed 1998). We see no substantive difference between the two views, particularly when one takes a Bayesian perspective, in which case the spatial term is seen as a random spatial process with a prior distribution.

While models of the form (1) have a simple structure, fitting them can be difficult for non-Gaussian responses. If the response were Gaussian, there are many methods, both classical and Bayesian, for estimating $\boldsymbol{\beta}$, $g(\cdot)$, and $\boldsymbol{\theta}$.

Most methods rely on integrating $g(\cdot)$ out of the model to produce a marginal likelihood or posterior. In the non-Gaussian case, this integration cannot be done analytically, which leads to substantial difficulty in fitting the model because of the high dimensional quantities that need to be estimated. Initial efforts to fit similar models have focused on approximating the integral in the GLMM framework or fitting the model in a Bayesian fashion. In the case of binary data, the approximations used in the GLMM framework may be poor (Breslow 2003) and standard Markov chain Monte Carlo (MCMC) techniques for the Bayesian model exhibit slow mixing (Christensen, Roberts, and Sköld 2005). More recent efforts have attempted to overcome these difficulties; this paper focuses on comparing promising methods and making recommendations relevant to practitioners.

Our goal in this paper is to investigate methods for fitting models of the form (1). We describe a set of methods (Section 3) that hold promise for good performance with Bernoulli and other non-Gaussian data and large samples (hundreds to thousands of individuals) and detail their implementation in Section 4. One of these methods, the spectral basis approach of Wikle (2002), has seen limited use; we develop the approach in this context by simplifying the model structure and devising an effective MCMC sampling scheme. We compare the performance of the methods on simulated epidemiological data (Section 5) as well as preliminary data from the Taiwan case-control study (Section 6). In evaluating the methods, our primary criteria are the accuracy of the fit, speed of the fitting method, and ease of implementation, including the availability of software. We close by discussing extensions of the models considered here and considering the relative merits and shared limitations of the methods.

3 Overview of methods

The methods to be discussed fall into two categories: penalized likelihood models fit via iteratively weighted least squares and Bayesian models fit via MCMC, but there are connections between all of them. First we describe two penalized likelihood methods, one in which the objective function arises from an approximation to the marginal likelihood in a mixed effects model, and a second in which the penalized likelihood is the original objective function of interest. Next we present several Bayesian methods, all of which use basis function representations of the spatial effect. Two of the methods (one penalized likelihood and one Bayesian) are motivated by the random effects framework, but can also be viewed as basis function representations of a regression term. We close the section by briefly mentioning some other methods of less promise for our purposes.

For both penalized likelihood and Bayesian models, in the Gaussian response setting, the unknown spatial function can be integrated out of the model. This integration leaves a small number of parameters to be estimated based on the marginal likelihood or marginal posterior, often using numerical maximization or MCMC. In a generalized model such as (1), fitting the model is difficult because the spatial process, or equivalently the basis coefficients or random

effects, cannot be integrated out of the model in closed form; estimating the high-dimensional quantities in the model poses problems for both penalized likelihood and Bayesian approaches. At their core, both of the penalized likelihood methods described here use iterative weighted fitting approaches to optimize the objective function. In the Bayesian methods, the spatial function is represented by a basis function representation and fit via MCMC; in some cases this representation is an approximation of a Gaussian process (GP). The methods employ a variety of parameterizations and computational tricks to improve computational efficiency.

To simplify the notation we use \mathbf{g}_s to denote the vector of values calculated by evaluating $g(\cdot)$ for each of the elements of \mathbf{s} (i.e., for each observation location), namely $\mathbf{g}_s = (g(\mathbf{s}_1), \dots, g(\mathbf{s}_n))^T$.

3.1 Penalized likelihood-based methods

3.1.1 Penalized likelihood and GLMMs

When the spatial function is represented as a random effects term, $\mathbf{g}_s = \mathbf{Z}\mathbf{u}$, model (1) is an example of a GLMM, with the variance of the random effects serving to penalize complex functions. Kammann and Wand (2003) recommend specifying \mathbf{Z} and $\text{Cov}(\mathbf{u}) = \Sigma$ such that $\text{Cov}(\mathbf{Z}\mathbf{u}) = \mathbf{Z}\Sigma\mathbf{Z}^T$ is a reasonable approximation of the spatial covariance structure of \mathbf{g}_s for the problem at hand. Kammann and Wand (2003) suggest constructing \mathbf{Z} based on the Matérn covariance, which takes the form,

$$C(\tau) = \frac{1}{\Gamma(\nu)2^{\nu-1}} \left(\frac{2\sqrt{\nu}\tau}{\rho} \right)^\nu \mathcal{K}_\nu \left(\frac{2\sqrt{\nu}\tau}{\rho} \right), \quad (2)$$

where τ is distance, ρ is the range (correlation decay) parameter, and $\mathcal{K}_\nu(\cdot)$ is the modified Bessel function of the second kind, whose order is the differentiability parameter, $\nu > 0$. This covariance function has the desirable property that sample functions of GPs parameterized with the covariance are $\lfloor \nu - 1 \rfloor$ times differentiable. As $\nu \rightarrow \infty$, the Matérn approaches the squared exponential form, with infinitely many sample path derivatives, while for $\nu = 0.5$, the Matérn takes the exponential form with no sample path derivatives. Ngo and Wand (2004) suggest basing \mathbf{Z} on the generalized covariance function corresponding to thin plate spline regression (see section 3.1.2 for details on this generalized covariance). Both approaches take $\Sigma = \sigma_u^2 \mathbf{I}$. \mathbf{Z} is constructed as $\mathbf{Z} = \Psi\Omega^{-\frac{1}{2}}$, where the elements of Ψ are the (generalized) covariances between the data locations and the locations of a set of pre-specified knots, κ_k , $k = 1, \dots, K$,

$$\Psi = (C(\|\mathbf{s}_i - \kappa_k\|))_{i=1, \dots, n; k=1, \dots, K}.$$

The matrix Ω has a similar form, but with pairwise (generalized) covariances amongst the knot locations. Kammann and Wand (2003) call this approach low-rank kriging because it is based on a parsimonious set of $K < n$ knots, which reduces the computational burden. This parameterization can be motivated by noticing that if a knot is placed at each data point and the basis coefficients are taken to be normal, then $\mathbf{g}_s = \mathbf{Z}\mathbf{u} \sim \mathbf{N}(\mathbf{0}, \sigma_u^2 \mathbf{C}) \Rightarrow g(\cdot) \sim \text{GP}(0, \sigma_u^2 \mathbf{C}(\cdot, \cdot))$;

i.e., $g(\cdot)$ has a GP prior distribution whose (generalized) covariance function, $C(\cdot, \cdot)$, is the covariance used in calculating the elements of Ψ and Ω . Fixing Z in advance forces σ_u^2 to control the amount of smoothing, allowing the model to be fit using standard mixed model software; for this reason Kammann and Wand (2003) fix ρ and ν in advance. Whether this overly constrains model fitting remains an open question, on which we touch in the discussion. One can also think of the GLMM representation as a radial (i.e., isotropic) basis representation for the spatial surface, with coefficients, \mathbf{u} , and basis matrix, Z .

Representing the spatial model as a GLMM seemingly makes available the variety of fitting methods devised for GLMMs, but many of these are not feasible for the high-dimensional integrals involved in spatial models. Most GLMM research that explicitly considers spatial covariates focuses on Markov random field (MRF) approaches to modelling the spatial correlation based on areal data (e.g., Breslow and Clayton 1993; Fahrmeir and Lang 2001; Banerjee et al. 2004), but this structure is not appropriate for individual-based data. Instead we use the penalized quasi-likelihood (PQL) approach of Breslow and Clayton (1993) and Wolfinger and O’Connell (1993), who arrived independently at an iterative weighted least squares (IWLS) procedure for fitting GLMMs, maximizing the objective function,

$$-\frac{1}{2\phi} \sum_{i=1}^n d_i(y_i, g(\mathbf{x}_i, \mathbf{s}_i)) - \frac{1}{2} \mathbf{u}^T \Sigma^{-1} \mathbf{u}, \quad (3)$$

where ϕ is a dispersion parameter and $d_i(\cdot)$ is the deviance, the log-likelihood up to a constant. REML is used to re-estimate the variance component(s) at each iteration. The approximations involved in arriving at the objective function (3) are generally thought to be poor for clustered binary data, resulting in biased estimates (Breslow 2003), though there is evidence that the method works well in the spatial setting (Hobert and Wand 2000; Wager, Coull, and Lange 2004), where the GLMM setup is merely a computational tool allowing estimation using mixed effects model software. The crux of the matter lies not in the accuracy of the approximation of the true integrated likelihood by (3), but in the appropriateness of (3) as a penalized log-likelihood objective function, in particular the form of the penalty term, the adequacy of REML in estimating the penalty (variance component) with binary data, and the performance of IWLS with the nested REML step.

3.1.2 Penalized likelihood and generalized cross-validation

Wood (2000, 2003, 2004) also proposes iterative weighted fitting of reduced rank thin plate splines with estimation of a smoothing parameter at each iteration, but he uses a different computational approach. Thin-plate splines are higher-dimensional extensions of smoothing splines and can be seen as a special case of a Gaussian process model, with generalized covariance (Cressie 1993, p. 303; O’Connell and Wolfinger 1997) characterized in terms of distance, τ , whose form in two dimensions is

$$C(\tau) \propto \tau^{2m-2} \log(\tau),$$

where m is the order of the spline (commonly two, giving an L_2 penalty).

For computational efficiency, Wood (2003) approximates the thin plate spline generalized covariance basis matrix, \mathbf{Z} , by a truncated eigendecomposition, \mathbf{Z}_k , which gives the following form for the spatial function,

$$g(\mathbf{s}_i) = \phi_i^T \boldsymbol{\alpha} + \mathbf{z}_{i,k}^T \mathbf{u},$$

where $\phi_i^T \boldsymbol{\alpha}$ are unpenalized polynomial terms. The method then optimizes a penalized log-likelihood with penalty term, $\lambda \mathbf{u}^T \mathbf{Z}_k \mathbf{u}$. The penalized log-likelihood objective function is similar to the GLMM objective function (3), and is also maximized using penalized IWLS, but with the smoothing penalty, λ , optimized at each iteration by an efficient generalized cross-validation (GCV) method (Wood 2000). The similarities between this approach and the GLMM approach suggest that they may give similar answers, as indeed appears to be the case in Section 5.3.1. One difference is that the GLMM spatial model uses a set of knots to reduce the rank of \mathbf{Z} , whereas the eigendecomposition is used here (but note that the number of knots can also be restricted in this approach). A second difference is the use of GCV rather than REML to estimate the smoothing parameter at each iteration. As with the GLMM approach the important estimation issues include the performance of the GCV criteria chosen to optimize the penalty term and the numerical performance of the iterative algorithm with nested penalty optimization.

3.2 Bayesian methods

In most Bayesian models, the spatial function is represented as a Gaussian process or by a basis function representation. Diggle et al. (1998) introduced generalized geostatistical models, with a latent Gaussian spatial process, as the natural extension of kriging models to exponential family responses. They used Bayesian estimation, suggesting a Metropolis-Hastings implementation, with the spatial function sampled sequentially at each observation location at each MCMC iteration. However, as shown in their examples and discussed elsewhere (Christensen, Møller, and Waagepetersen 2000; Christensen and Waagepetersen 2002; Christensen et al. 2005), this implementation is slow to converge and mix, as well as being computationally inefficient because of the inverse covariance matrix involved in calculating the prior for \mathbf{g}_s .

An alternative approach, which avoids large matrix inversions, is to express the unknown function in a basis, $\mathbf{g}_s = \mathbf{Z}\mathbf{u}$, where \mathbf{Z} contains the basis function values evaluated at the locations of interest, and estimate the basis coefficients, \mathbf{u} . When the coefficients are normally distributed, this representation can be viewed as a GP evaluated at a finite set of locations, with $\text{Cov}(\mathbf{g}_s) = \mathbf{Z}\text{Cov}(\mathbf{u})\mathbf{Z}^T$. Two of the methods described below use such basis function approximations to a stationary GP, while the third, a neural network model, relies on a basis function representation that, while not explicitly designed to approximate a particular stationary GP, does give an implicit GP prior distribution for the spatial process, and has been shown to have a close connection to GP models (Neal 1996).

3.2.1 Bayesian GLMMs

Zhao and Wand (2005) model the spatial function by approximating a stationary GP using the basis function representation, $\mathbf{g}_s = \mathbf{Z}\mathbf{u}$, given in the penalized likelihood setting in Section 3.1.1. They specify a Bayesian model, with $\mathbf{u} \sim N(0, \sigma_u^2 \mathbf{I})$, the prior distribution over the basis coefficients, and fit the model via MCMC. As suggested in Kammann and Wand (2003), Zhao and Wand (2005) fix the covariance parameters, taking $\nu = 1.5$ and

$$\rho = \max_{i,j=1,\dots,n} \|\mathbf{s}_i - \mathbf{s}_j\|,$$

and letting the variance parameter σ_u^2 control the degree of smoothing. One could estimate ρ and ν in the MCMC, as well as include anisotropy parameters in the covariance calculations, but this would require recalculating Ψ and $\Omega^{-\frac{1}{2}}$ at each iteration, which would slow the fitting process and likely produce slower mixing.

3.2.2 Bayesian spectral basis representation

A second method that improves computational efficiency by using basis functions to approximate a stationary GP is a spectral, or Fourier, representation. Isotropic GPs can be represented in the Fourier basis, which allows one to use the Fast Fourier Transform (FFT) to speed calculations. Here we describe the basic approach in two-dimensional space, following Wikle (2002); we leave the details of our implementation to Section 4.4, with further description of the spectral basis construction in the appendix.

The key to the spectral approach is to approximate the function $g(\cdot)$ on a grid, $\mathbf{s}^\#$, of size $K = k_1 \times k_2$, where k_1 and k_2 are powers of two. Evaluated at the grid points, the vector of function values is represented as

$$\mathbf{g}_{\mathbf{s}^\#} = \mathbf{Z}\mathbf{u}, \tag{4}$$

where \mathbf{Z} is a matrix of orthogonal spectral basis functions, and \mathbf{u} is a vector of complex-valued basis coefficients, $u_m = a_m + b_m i$, $m = 1, \dots, K$. The spectral basis functions are complex exponential functions, i.e., sinusoidal functions of particular frequencies; constraints on the coefficients ensure that $\mathbf{g}_{\mathbf{s}^\#}$ is real-valued and can be expressed equivalently as a sum of sine and cosine functions. To approximate mean zero stationary GPs, the basis coefficients have the prior distribution,

$$\begin{pmatrix} \mathbf{a} \\ \mathbf{b} \end{pmatrix} \sim N(\mathbf{0}, \Sigma_\theta) \tag{5}$$

where the diagonal (asymptotically, see Shumway and Stoffer (2000, Section T3.12)) covariance matrix of the basis coefficients, Σ_θ , parameterized by θ , can be expressed in closed form (for certain covariance functions) using the spectral density of the GP covariance function. In particular, we follow Wikle (2002) in using the popular Matérn

covariance (2), whose spectral density function, evaluated at spectral frequency $\boldsymbol{\omega}$, is

$$f_{(\rho,\nu)}(\boldsymbol{\omega}) = \frac{\Gamma(\nu + \frac{d}{2})(4\nu)^\nu}{\pi^{\frac{d}{2}}\Gamma(\nu)(\pi\rho)^{2\nu}} \cdot \left(\frac{4\nu}{(\pi\rho)^2} + \boldsymbol{\omega}^T \boldsymbol{\omega} \right)^{-(\nu + \frac{d}{2})}, \quad (6)$$

where d is the dimension of the space (two in this case). For an appropriate set of spectral frequencies, the diagonal elements of $\boldsymbol{\Sigma}_\theta$ are the values of $f_{(\rho,\nu)}(\cdot)$ at those frequencies, and the off-diagonals are zero. The process at the observation locations is calculated through an incidence matrix, \mathbf{P} , which maps each observation location to the nearest grid location, and σ , the standard deviation of the process,

$$\mathbf{g}_s = \sigma \mathbf{P} \mathbf{g}_{s\#}. \quad (7)$$

For a fine grid, the error induced in associating observations with grid locations should be negligible and the piecewise constant representation of the surface tolerable. The computational efficiency comes in the fact that the matrix \mathbf{Z} , which is $K \times K$, need never be explicitly formed, and the operation $\mathbf{Z}\mathbf{u}$ is the inverse FFT, and so can be done very efficiently ($O(K \log_2 K)$). In addition, evaluating the prior for \mathbf{u} is fast because the coefficients are independent a priori. This stands in contrast to the standard MCMC setup for GP models, in which the prior on \mathbf{g}_s involves $O(n^3)$ operations with an $n \times n$ matrix. The number of observations affects the calculations only through the likelihood, which scales as $O(n)$, because the observations are independent conditional on \mathbf{g}_s . In fact, a dataset with 10000 observations took only twice as long to fit via MCMC as a dataset with 1200 observations.

3.2.3 Bayesian neural network

The final method, a neural network model, is also a basis function method, in which the basis functions, as well as their coefficients, are sampled during the MCMC. The particular neural network model we consider is a multilayer perceptron (MLP), with one hidden layer. A common form of this model specifies the spatial process,

$$g(\mathbf{s}_i) = \mu + \sum_{k=1}^K z_k \left(\boldsymbol{\theta}_k^T \mathbf{s}_i \right) u_k,$$

where $z(\cdot)$ is commonly chosen to be the logistic (sigmoid) or tanh function and the $\boldsymbol{\theta}_k$ parameters determine the position and orientation of the basis functions. One can think of the MLP model as basis function regression in which the position of the k th basis function changes as $\boldsymbol{\theta}_k$ changes. One drawback to fitting neural network models in a likelihood framework is the multimodality of the likelihood (Lee 2004); recent work has focused on specifying Bayesian neural network models and fitting the models via MCMC (Neal 1996; Lee 2004).

3.3 Other methods

There are many methods designed for spatial data, usually for Gaussian responses, and for nonparametric regression in general. In principle, most or all could be adapted for binary spatial data, but they would raise many of the fitting

issues already discussed in this paper. We mention a few of the methods here, but do not include them in the empirical comparison because they lack readily available code or would need extensive further development for application to binary spatial data.

In contrast to the approximation to the integral involved in the PQL approach, several papers have provided EM (McCulloch 1994, 1997; Booth and Hobert 1999), numerical integration (Hedeker and Gibbons 1994; Gibbons and Hedeker 1997), and MCMC (Christensen 2004) methods for maximizing the GLMM likelihood. However, software for the approaches does not seem to be available, and the algorithms are complex and computationally intensive; we do not consider these to be currently viable methods for practitioners. Wahba, Wang, Gu, Klein, and Klein (1995) represent nonparametric functions as ANOVA-like sums of smoothing splines and optimize a penalized log-likelihood in an iterative fashion, similar to the penalized methods described previously. However, as noted by Wood (2004), the approach generally requires a parameter per data point, making computations inefficient, and the only available software is a set of Fortran routines, which are less user-friendly than desired here. The Bernoulli likelihood (1) can be expressed using data augmentation in a way that allows for Gibbs sampling (Albert and Chib 1993) as the MCMC technique, but the computations involve $n \times n$ matrices at each iteration. Holmes and Mallick (2003) extend the free-knot spline approach of Denison, Holmes, Mallick, and Smith (2002) to generalized regression models. They fit the model via reversible-jump MCMC and have software for the Gaussian model, but software for the generalized model was not available. For nonstationary Gaussian data, authors have used mixture models, including mixture of splines (Wood, Jiang, and Tanner 2002) and mixture of Gaussian processes (Rasmussen and Ghahramani 2002), in which the mixture weights depend on the covariates (the spatial locations in our context), but this adds even more complexity to MCMC implementations and has not been developed for the generalized model. Finally, Christensen et al. (2005) develop a data-dependent reparameterization scheme for improved MCMC performance and apply the approach with Langevin updates that use gradient information; while promising, the approach is computationally intensive, again involving $n \times n$ matrix computations at each iteration, and software is not available.

4 Implementation

Here we describe the implementation of each method, coded in R with the exception of the neural network, with descriptions of the prior distributions and MCMC sampling schemes for the Bayesian models. The subsection headings indicate the abbreviations we use to denote the methods in discussing the results.

4.1 Penalized likelihood and GLMMs (PL-PQL)

We follow the basic approach of Ngo and Wand (2004), using the thin plate spline basis and estimating the penalized likelihood model via the PQL approach. This can be performed with standard software by iteratively calling a mixed model fitting routine designed for Gaussian responses. The SemiPar library in R (released after our simulations were conducted) fits the model as does the `gamm()` function in the `mgcv` library; we used the `glmmPQL()` function in R. We use an equally-spaced 8×8 grid of knot locations; using a 16×16 grid had little effect on our empirical results in a sensitivity assessment. Additional covariates can be included in a linear or smooth manner as described in Ngo and Wand (2004). Prediction at unobserved locations is done efficiently using the estimated basis coefficients, \mathbf{u} , and a prediction basis matrix, \mathbf{Z}_{pred} , constructed in the same way as \mathbf{Z} but with Ψ_{pred} containing the pairwise covariances between the knot locations and the prediction locations. The SemiPar library provides uncertainty estimates.

We also ran the model with the Matérn covariance with fixed range and smoothness parameters, as suggested by Kammann and Wand (2003), and found that the results varied depending on the value of the range parameter. For the isotropic dataset, using the value of $\rho = \max \|s_i - s_j\|$, the method performed markedly worse than with the thin plate spline covariance, while choosing a value of ρ equal to one-fourth the recommended value produced results similar to the thin plate spline-based model. This suggests that the method is sensitive to the range parameter, but note Zhang (2004), who shows that σ^2 and ρ cannot both be estimated consistently.

4.2 Penalized likelihood and GCV (PL-GCV)

We used the `gam()` function from the `mgcv` library in R to fit the penalized likelihood model based on GCV, using the default of a $k = 30$ dimensional basis, which appeared to be sufficient for our simulations and data. The approach can handle additional covariates in a linear or smooth manner. The `mgcv` library provides predictions at unobserved locations and uncertainty estimates for parameters and the spatial field; there is a brief discussion of these uncertainty estimates for the generalized model in Wood (2003). One drawback, shared by most of the other methods, is that the method, as implemented in R, is not designed for anisotropy. In principle this could be handled using additional smoothing parameters (Wood 2000); Wood (2003) mentions that work is in progress.

4.3 Bayesian GLMM (Geo)

For the Bayesian version of the GLMM approach, we follow Zhao and Wand (2005) but modify the approach to improve MCMC performance. Zhao and Wand (2005) use vague proper Gaussian priors for the fixed effect coefficients, β , ($\sigma_\beta^2 = 10^{10}$) and a vague inverse-gamma prior for the variance component, $\sigma_u^2 \sim \text{IG}(a = 0.5, b = 0.0005)$, with mean $b/(a - 1)$ (for $a > 1$). They fit the model via MCMC using Metropolis-Hastings with t-distributed joint propos-

als of the weighted least squares type for the coefficients (β, \mathbf{u}) , as suggested by Gamerman (1997), and conjugate Gibbs sample updates for $\sigma_{\mathbf{u}}^2$.

We tried this MCMC scheme, but made several changes to improve mixing; even with these changes, the scheme did not perform as well as the spectral basis approach (Section 5.3.2). First, we found that t -distribution proposals for the coefficients were rarely accepted because of the high variability in the proposals; we used a multivariate normal proposal density with the same form for the mean and covariance (scale) matrix as Zhao and Wand (2005), but with the covariance matrix multiplied by a tuneable constant, w , to achieve acceptance rates of approximately 0.22 for the coefficients. Rather than sampling β and \mathbf{u} together, we separately sampled β using a simple Metropolis proposal. Second, we found that the critical smoothing parameter, $\sigma_{\mathbf{u}}^2$, mixed very slowly when sampled via conjugate Gibbs updates, because of the strong dependence between $\sigma_{\mathbf{u}}^2$ and \mathbf{u} . Instead, following Paciorek (2003), we sampled $\sigma_{\mathbf{u}}$ jointly with the coefficients, \mathbf{u} . As the first part of the joint sample, we sampled $\sigma_{\mathbf{u}}$ using a Metropolis scheme. Then, conditional on the proposed value of $\sigma_{\mathbf{u}}$, we sampled \mathbf{u} using the multivariate normal proposal density used for sampling \mathbf{u} , described above, with $w = 1$. Our prior for $\sigma_{\mathbf{u}}$ was $N(0, 1000)$, left-truncated at 0.001, with a normal proposal distribution centered on the current value. Sampling $\sigma_{\mathbf{u}}$ directly, rather than on the log scale, allowed us to use the same proposal variance for all values of the parameter. We suspect that slice sampling would work well for this parameter, but that it should still be employed in a joint sample of $\sigma_{\mathbf{u}}$ and \mathbf{u} .

We used an equally-spaced 8×8 grid of knot locations; using a 16×16 grid had little effect on our empirical results in a sensitivity assessment. Prediction is done efficiently at each iteration in the same way as described in Section 4.1. As described in Zhao and Wand (2005), additional smooth covariate terms can be included in the model and fit in similar fashion to the spatial term.

Note that we did not apply this method to the 10000 observation cohort simulation because the multivariate proposal density of Zhao and Wand (2005) involves matrix multiplications with K by n and n by n matrices. An alternative approach in which the K basis coefficients were proposed as a vector, but independently, would be substantially more efficient, but would likely show slower mixing than the proposal used here.

4.4 Bayesian spectral basis (SB)

This approach is based on Wikle (2002) with modifications for this context and a custom sampling scheme. Wikle (2002) embeds the spectral basis representation (4.7) in a hierarchical model that involves several error components, including one relating \mathbf{g}_s to the likelihood and one relating $\mathbf{Z}\mathbf{u}$ to $\mathbf{g}_{s\#}$. Our model omits these additional error components, both for simplicity and because the modification allows for reasonably fast MCMC mixing; the fact that the basis coefficients directly involved in the likelihood (1), rather than further from the data in the hierarchy of the model may help with mixing. In addition to the likelihood (1) and the prior on \mathbf{u} (5), we need only specify priors

on β , σ , ρ , and ν . These are taken to be proper but non-informative. In particular, for binary data with no additional covariates, we take $\beta_0 \sim N(0, 10)$, $\log \sigma \sim N(0, 9)$, and $\nu \sim U(0.5, 30)$. For ρ , we use a prior that favors smoother surfaces, taking $\zeta = \log \rho$ and $f(\zeta) \propto \zeta^2 I(\zeta \in (-4.6, 1.35))$. The exact form of this prior is not critical, except that forcing the range parameter to remain in the interval is important for preventing it from wandering in extreme parts of the space in which it has little effect on the likelihood.

For β and $\log \sigma$ we use Metropolis and Metropolis-Hastings proposals, respectively. We propose each of $\log \rho$ and ν jointly with \mathbf{u} . First we propose $\log \rho$ or ν using Metropolis-Hastings or Metropolis proposals, respectively. Then, conditional on the proposed hyperparameter, we propose

$$u_i^* = u_i \cdot \frac{\sqrt{(\Sigma_{\theta^*})_{i,i}}}{\sqrt{(\Sigma_{\theta})_{i,i}}}, \quad i = 1, \dots, K,$$

where $\theta^* = (\rho^*, \nu)$ or $\theta^* = (\rho, \nu^*)$ depending on which hyperparameter is being proposed. Modifying u_i based on its prior variance, $(\Sigma_{\theta})_{i,i}$, allows the covariance hyperparameters to mix more quickly by avoiding proposals for which the coefficients are no longer probable based on their new prior variances. Such a deterministic proposal for \mathbf{u} is a valid MCMC proposal so long as the Jacobian of the transformation is included in the acceptance ratio, based on a modification of the argument in Green (1995). Both σ and $\log \rho$ require Metropolis-Hastings sampling with the proposal variances depending on the parameter value to achieve constant acceptance rates; slice sampling may be a superior alternative for these parameters, allowing the proposal variance to adjust to the parameter value. As described in the appendix, the spectral basis coefficients, \mathbf{u} , are sampled in blocks (grouped according to their corresponding frequencies) via Metropolis proposals.

We use a grid, $\mathbf{s}^\#$, of size 64×64 , but as noted in the appendix, this corresponds to an effective grid of 33×33 . Code for implementing the model in R is given in the electronic supplement. Additional linear covariates can be easily included, while smooth covariate terms can be included in the model using the spectral basis representation (see also Lenk (1999)). If one wants to avoid the discretization, one might use the mixed model approach of Zhao and Wand (2005), among other possibilities. Prediction, done at the grid locations, is implicit in the estimation of $\mathbf{g}_{\mathbf{s}^\#}$.

4.5 Bayesian neural network (NN)

We use the Flexible Bayesian Modeling software of R. Neal (<http://www.cs.toronto.edu/~radford/fbm.software.html>); this software uses tanh functions for $z_k(\cdot)$ and vague, proper priors for the various hyperparameters, with MCMC sampling done via a combination of Gibbs sampling and hybrid Monte Carlo. We use the default prior specification given in the binary regression example in the software's documentation. We fix the number of hidden units at a relatively large value, $K = 50$, to allow for a sufficiently flexible function but minimize computational difficulties.

5 Simulations

We evaluate the methods on four simulated datasets, allowing us to assess the methods in a variety of situations that are likely to arise in practice. The simulations allow us to explore estimation under basic spatial structures plausible for large epidemiological datasets, in particular contrasting a constant spatial surface with surfaces with single peaks. Without further simulations, we do not know if the results would generalize to surfaces with multiple peaks, but since epidemiological investigations often have insufficient power to detect any spatial heterogeneity, our simulations are a good starting point. To focus on the spatial structure, we include only a mean and no covariates as the $X\beta$ portion of the model.

We assess the performance of the methods in estimating the known spatial surfaces, their computational speed, and MCMC convergence for the Bayesian methods.

5.1 Datasets

The first three datasets mimic case-control data similar to those of the Taiwan example. The first dataset has no spatial effect. The second has a point source-induced isotropic spatial effect with a single maximum in the risk (probability) surface. The third has a point source-induced spatial effect with anisotropy to simulate the effect of prevailing winds. The spatial domain of all three datasets is a square area 15 units on a side, and the baseline risk of disease is 0.0003. For the latter two datasets, the exposure peak occurs at the middle of the square and the risk there is four times the baseline risk. For the isotropic surface, the risk drops off following a bivariate normal distribution with standard deviations of 1.5 and correlation of zero, while for the anisotropic surface, the risk drops off following a bivariate normal with standard deviations of 3.75 and covariance of $0.8 \cdot 3.75$. Sampling mimics a case-control study. First, a population of individuals is located randomly in the area. Based on the underlying risk surface, each individual is randomly assigned to have a health outcome or not. $n_1 = 200$ cases and $n_0 = 1000$ controls are then randomly selected from the populations of affected and unaffected individuals. The fourth dataset mimics a cohort study in which a group of individuals are followed over time to determine which individuals develop disease. We select 10000 individuals randomly from a metropolitan area of size 50 km by 50 km. There are four concentric squares (50 km by 50 km, 19 by 19, 9 by 9, and 3 by 3) with population density increasing toward the middle of the area from 500 individuals per square km in the outermost region to 3000, 7000, and finally 10000 in the inner square and corresponding increasing risk of 0.10, 0.11, 0.12, and 0.13.

For each dataset, with fixed underlying spatial risk function, we evaluate each method on 50 data samples in which the locations and health outcomes of individuals are sampled.

5.2 Assessment

In the case-control setting, the methods calculate $\hat{p}(s_i)$. This estimates the risk surface at a location conditional on inclusion (indicated by $\Delta_i = 1$) in the study, $\check{p}_{\text{COND}}(s_i) = P(Y_i = 1 | s_i, \Delta_i = 1)$, rather than the true marginal risk surface, $\check{p}_{\text{MARG}}(s_i) = P(Y_i = 1 | s_i)$, given in Section 5.1. The conditional and marginal risk surfaces are offset by a constant on the logit scale (Carroll et al. 1995, p.184; Elliott et al. 2000). To assess the accuracy of the conditional surfaces estimated by the methods, we compute the true value of the conditional risk surface, $\check{p}_{\text{COND}}(s_i) = \check{p}_{\text{MARG}}(s_i) + \log r$, where $r = (n_1(1 - P(Y_i = 1)))/(n_0 P(Y_i = 1))$ is the relative sampling intensity of cases and controls. Henceforth we refer only to the conditional risk surfaces, dropping the subscript, C, and considering the surface at a grid of test locations, $p_m = p(s_m^*)$, $m = 1, \dots, M$.

We use several criteria to compare the fits from the various methods. The first is the mean squared error, $\text{MSE}_{\text{sim}} = M^{-1} \sum_{m=1}^M (\check{p}_m - \hat{p}_m)^2$, where for the Bayesian models, \hat{p} is the posterior mean. MSE is not really appropriate for probabilities; a measure based on predictive density is more principled, so the second measure uses the Kullback-Leibler (KL) divergence between the predictive density of test data given the fitted surface, $h(y_m^* | \hat{p}_m)$, and the true density, $h(y_m^* | \check{p}_m)$, where the integral over the true Bernoulli distribution of observations at location m , $H(y_m^* | \check{p}_m)$, is averaged over the grid of test locations,

$$\begin{aligned} \text{KL}_{\text{sim,point}} &= \frac{1}{M} \sum_{m=1}^M \int \log \frac{h(y_m^* | \check{p}_m)}{h(y_m^* | \hat{p}_m)} dH(y_m^* | \check{p}_m) \\ &= \frac{1}{M} \sum_{m=1}^M \left(\check{p}_m \log \frac{\check{p}_m}{\hat{p}_m} + (1 - \check{p}_m) \log \frac{1 - \check{p}_m}{1 - \hat{p}_m} \right). \end{aligned}$$

With the Bayesian approaches, we can also use the full posterior, averaging over the MCMC samples, $t = 1, \dots, T$, to assess fit for a vector of test data, $\mathbf{y}^* = (y_1^*, \dots, y_M^*)$, again using the KL divergence, and scaling by M ,

$$\text{KL}_{\text{sim,Bayes}} = \frac{1}{M} \int \log \frac{h(\mathbf{y}^* | \check{\mathbf{p}})}{h(\mathbf{y}^* | \hat{\mathbf{p}})} dH(\mathbf{y}^* | \check{\mathbf{p}}) \quad (8)$$

$$\approx \frac{1}{M} \log \frac{h(\mathbf{y}^* | \check{\mathbf{p}})}{h(\mathbf{y}^* | \hat{\mathbf{p}})} \quad (9)$$

$$= \frac{1}{M} \log \frac{h(\mathbf{y}^* | \check{\mathbf{p}})}{\int h(\mathbf{y}^* | \mathbf{p}) \Pi(\mathbf{p} | \mathbf{y}) d\mathbf{p}} \quad (10)$$

$$\approx \frac{1}{M} \sum_{m=1}^M (y_m^* \log \check{p}_m + (1 - y_m^*) \log(1 - \check{p}_m)) \quad (11)$$

$$- \frac{1}{M} \log \frac{1}{T} \sum_{t=1}^T \prod_{m=1}^M p_{m,(t)}^{y_m^*} (1 - p_{m,(t)})^{1 - y_m^*}. \quad (12)$$

Note that the resulting quantity (11-12) calculates the predictive density of the test data (12) (the conditional predictive ordinate approach of Carlin and Louis (2000, p. 220)) under each method relative to the predictive density of the test



data under the true distribution (11). Ideally, this calculation should average over many samples of test data, \mathbf{y}^* (8), but we use only one for computational convenience (9). However, note that the assessment over a large test set taken at many locations, M , allows the variability over locations to stand in for the variability over test samples and that we compute $\text{KL}_{\text{sim, Bayes}}$ for each of 50 data samples from each dataset.

To assess the uncertainty estimates of the methods, we compare the length and coverage of 95% confidence and credible intervals over the true function values at the test locations. For PL-GCV, we calculate the confidence intervals using 1.96 multiplied by the standard error from the `predict.gam()` function in the `mgcv` library. For the Bayesian methods, we use the 2.5 and 97.5 percentiles of the iterates from the Markov chains. Uncertainty estimates were not readily available for PL-PQL (but are now available through the `SemiPar` library) and NN, so we omitted them from this analysis.

For the Bayesian methods, since mixing and convergence have been problems, we also assess MCMC mixing speed. The different methods have different parameterizations, so this is largely qualitative, but we directly compare the samples of the log posterior density, $f(\boldsymbol{\theta}|\mathbf{y})$ (Cowles and Carlin 1996), examining the autocorrelation and effective sample size (Neal 1993, p. 105),

$$\text{ESS} = \frac{T}{1 + 2 \sum_{d=1}^{\infty} \rho_d(f(\boldsymbol{\theta}|\mathbf{y}))}, \quad (13)$$

where $\rho_d(f(\boldsymbol{\theta}|\mathbf{y}))$ is the autocorrelation at lag d for the log posterior, truncating the summation at the lesser of $d = 10000$ or the first d such that $\rho_d(\pi(\boldsymbol{\theta}|\mathbf{y})) < 0.05$. Since the real limitation is computational, we also estimate ESS per processor hour, to scale the methods relative to the speed of computing each iteration.

5.3 Results

5.3.1 Quality of fit

The spectral basis model provides the best compromise between sensitivity and specificity based on the simulations, as shown in Figure 1. For the null dataset with no spatial effect, we see that the SB and NN models are markedly better than the other models in terms of MSE and point estimate KL divergence (Fig. 1, row 1), as well as when comparing amongst Bayesian models based on the full KL divergence (not shown). NN outperforms SB, but both have MSE and KL divergence close to zero. The remaining models have MSE and KL far from zero, clearly overfitting by finding features in the spatial surface that do not exist (not shown). All differences are significant based on paired t-tests. We do not control for multiple testing as we merely wish to give a rough idea of the signal to noise ratio; in most cases here and below in which there are significant differences, the p-values are very small ($p < 0.001$).

The results for the isotropic and anisotropic case-control simulations (Figure 1, rows 2 and 3) show that NN avoids overfitting on the null dataset because it has little power to detect effects when they do exist. It has much

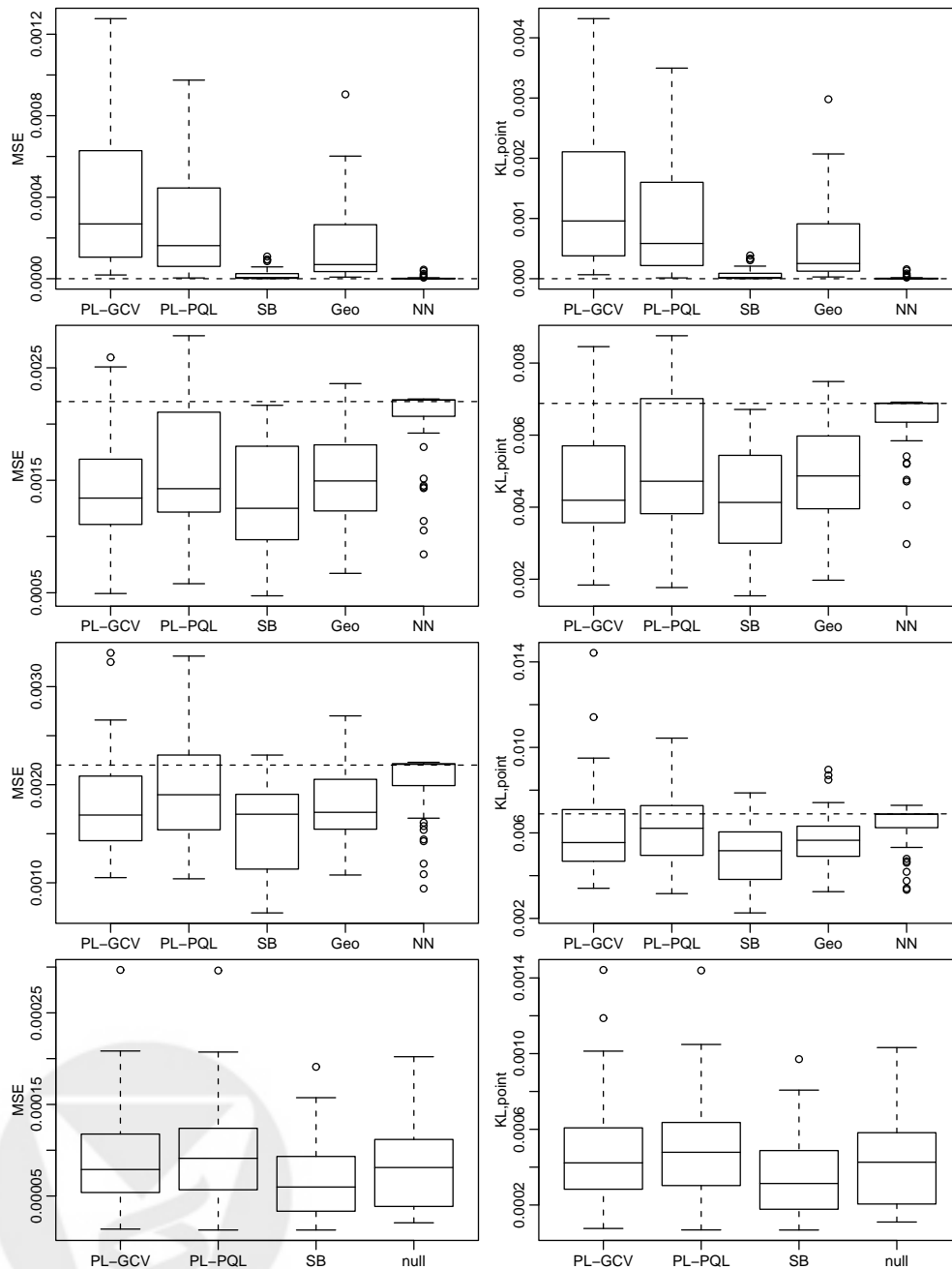


Figure 1. Test set MSE (left column) and point KL divergence (right column) from the five methods for 50 replicated data samples from each of four datasets: null (first row), isotropic (second row), anisotropic (third row), and cohort (fourth row). The dotted horizontal line is the criteria for a null model of $\hat{p}_0(\mathbf{s}_i) = \frac{n_1}{n_0+n_1}$. For the cohort simulation, we used only PL-GCV, PL-PQL, and SB; 'null' indicates the performance of a non-spatial null model, $\hat{p}(\mathbf{s}_i) = \bar{Y}$.

higher MSE and KL divergence than the other methods, approaching the MSE and KL divergence of the null model, $\hat{p}_0(\mathbf{s}_i) = \frac{n_1}{n_0+n_1} = \frac{1}{6}$. In contrast, SB performs as well as the best of the other methods (PL-GCV) on the isotropic dataset and outperforms all methods on the anisotropic dataset. On the isotropic dataset, SB is significantly better than PL-GCV for KL divergence ($p = 0.01$) but not for MSE ($p = 0.29$), while SB and PL-GCV are significantly better than the other methods except that PL-GCV and Geo are not significantly different for KL ($p = 0.18$). On the anisotropic dataset, SB is significantly better than the other methods, while PL-GCV is significantly better than PL-PQL ($p = 0.044$) and NN ($p = 0.015$), but not Geo ($p = 0.58$). Except as noted, $p < 0.0001$ for the SB method compared to the other methods.

For the simulated cohort study, we compare only the PL-GCV, PL-PQL, and SB methods because with $n = 10000$, the computations are too slow for the geoaddivitive model and the neural network. For this dataset, once again the spectral basis model outperforms the penalized likelihood methods ($p < 0.0001$), which are not significantly different (Figure 1, row 4). SB is also significantly better than a constant null model, $\hat{p}(\mathbf{s}_i) = \bar{Y}$, ($p < 0.00001$), while the penalized likelihood methods are not.

The uncertainty assessment indicates some differences between the methods (Table 1). On the flat dataset, all three methods have coverage higher than 95%, with the SB having the shortest intervals. On the isotropic and anisotropic datasets, the SB has longer intervals than Geo, but coverage is closer to 0.95. If one artificially scales the interval lengths to achieve 95% coverage, the lengths of the geoaddivitive intervals are longer than those of the spectral basis model. For the cohort study, both PL-GCV and SB undercover, with SB giving poorer coverage, but with shorter intervals. If one artificially scales the lengths, the SB intervals are shorter than those from PL-GCV. In general, with the exception of the cohort study, the SB model seems to perform better in terms of uncertainty estimation, giving coverage closer to the desired 95%, with either shorter intervals than the other methods, or intervals that are longer because of undercoverage by the other methods. The lengths of the intervals indicate the difficulty in drawing firm conclusions about small relative risks. In particular for the cohort study, in which the true risk varies between 0.10 and 0.13, interval lengths are in the vicinity of 0.03, suggesting that even with a cohort size of 10000, we will have difficulty detecting areas with increased risk with reasonable certainty.

5.3.2 Computational speed and MCMC performance

The penalized likelihood methods are much faster to fit than the spectral basis method, which is in turn faster than the geoaddivitive model and the neural network, using a Linux machine with a 3.06 GHz Intel Xeon (32 bit) processor and 2G of memory (Table 2). The speed advantage of SB relative to the other Bayesian models increases for larger datasets, because increasing the number of observations only changes the speed of the $O(n)$ likelihood evaluation in SB. Based on the log posterior, which exhibits less autocorrelation in SB than Geo (see below), the speed advantage

Table 1. Average coverage (interval length) of 95% confidence and credible intervals for the function values at 2500 test locations for the PL-GCV, SB, and Geo models, averaged over the 50 replicated data samples for each of the four datasets. Geo was not fit to the cohort dataset for computational reasons.

	PL-GCV	SB	Geo
null	0.983 (0.088)	1.000 (0.068)	0.999 (0.081)
isotropic	0.939 (0.133)	0.959 (0.131)	0.919 (0.109)
anisotropic	0.914 (0.135)	0.947 (0.133)	0.884 (0.110)
cohort	0.918 (0.0350)	0.870 (0.0285)	NA

is even more pronounced after adjusting for the effective sample size (13).

While a rapidly varying spatial surface would require a denser grid for the spectral basis, it would also require more knots for the geoadditive model and more hidden units for the neural network model, so the relative speeds of the Bayesian methods may not change substantially; all of the models would be slow to fit.

For certain models, memory use in R can be high, reaching 825M, 245M, and 384M for the PL-GCV, PL-PQL, and SB methods, respectively, on the cohort dataset. This may be a limitation on certain machines, but there are often tricks for reducing memory use; in the case of PL-GCV, one can specify a set of knots to reduce the memory usage.

Consistent with other reports in the literature (Christensen et al. 2005; Zhao and Wand 2005), all the Bayesian methods show slow mixing, despite our attempts to improve MCMC performance. The primary difficulty involves the correlation amongst the spatial function values and the strong relationship between the smoothing parameter(s) and the function values. Based on a long run (100,000 iterations) with one data sample from the isotropic dataset, the spectral basis model shows more rapid mixing of the smoothing parameters than the geoadditive model with effective sample sizes of 772 for σ and 316 for ρ for the spectral basis model compared to 93 for σ for the geoadditive model. In assessing the model as a whole through the log posterior, the effective sample size for the SB model is 397, somewhat better than 240 for the geoadditive model. Combined with the speed advantage per nominal iteration of the SB model, the computational efficiency of the SB model is much better than the geoadditive model.

It is difficult to assess the mixing of the neural network model, first because we can only extract the log likelihood and not the log posterior from the software, and second because the model generally fails to detect the structure in the data; good mixing for a posterior that doesn't fit the data is not particularly relevant.

Table 2. Computational speed for each of the methods for two different sample sizes, $n = 1200$ and $n = 10000$. For the Bayesian methods we provide the time expended per 1000 nominal iterations and per 1000 effective iterations, adjusting for the effective sample size (13) for the SB and Geo models. Note that for the NN, which uses hybrid Monte Carlo sampling, the number of leapfrog steps in a single iteration (we used 20) affects the time taken to perform one nominal iteration.

	n=1200	n=10000
PL-GCV	1.8s	93s
PL-PQL	6.5s	37s
SB (time/1000 iterations)	1.3m	3m
Geo (time/1000 iterations)	15m	not run
NN (time/1000 iterations)	5.5m	not run
SB (time/1000 effective it.)	6h	13h
Geo (time/1000 effective it.)	104h	not run

5.3.3 Ease of implementation

The penalized likelihood methods are the easiest to implement in terms of coding and software availability. In particular, the penalized thin plate spline of Wood (2003) is implemented in the `mgcv` package in R and can be fit with a few lines of code. The PL-PQL approach can be easily fit in R using the `SemiPar` library. The spectral basis and geoaddivitive models both require coding an MCMC algorithm, which is relatively complicated, although we provide template code in the electronic supplement and have posted an R library, `spectralGP`, that manipulates the spectral representation. The FBM software of R. Neal allows one to fit neural network models without writing code, but the prior specifications are difficult to understand and wrapper code (e.g., in Matlab or R) is needed to prepare the model and process the final chain. Also, only certain outputs from the chain are available.

6 Case study

6.1 Background and data

The Kaohsiung metropolitan area is a center of petrochemical production in Taiwan. Population density is high in the vicinity of four petroleum/petrochemical complexes, and data suggest that hydrocarbon and volatile organic compound concentrations are much higher than in industrialized areas in the United States, raising concern that the complexes may be causing adverse health effects. In particular, leukemia and brain cancer have been linked to exposure to

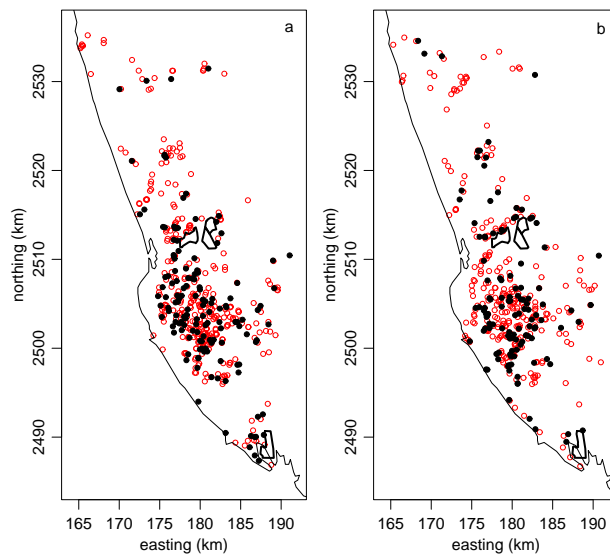


Figure 2. Locations of controls (open circles) and cases (closed circles) for (a) leukemia and (b) brain cancer in the Kaohsiung area. The boundaries of the four petrochemical complexes are indicated with thick lines and the coastline by a thin line.

pollutants from petrochemical production. A preliminary unpublished case-control study suggests that individuals less than 30 years old who live within three km of one of the four complexes have an increase in leukemia and brain neoplasms. An ongoing case-control investigation is designed to investigate whether proximity to the complexes is linked to leukemia and brain cancer.

While the actual study is ongoing, we analyze interim data to illustrate the methods. As we need a single location for each individual, we assigned each individual to the location at which they resided the longest in the time between birth and either age 30 or the present time for the controls and birth and diagnosis for the cases. We removed individuals whose location could not be geocoded and those living far from the center of Kaohsiung city, leaving 495 (433) individuals in the leukemia (brain cancer) analysis, of whom 141 (121) were diagnosed with leukemia (brain cancer). The small number of individuals living close to the petrochemical complexes (Fig. 2) suggests in advance that it will be difficult to detect any increase in risk arising from the complexes.

6.2 Assessment

To compare the methods, we divided both the brain cancer and leukemia datasets into 10 nearly equal size sets and sequentially held out each set as a test set. We compare amongst the methods and to a null model that estimates a

Table 3. Deviance summed across the 10 held-out sets for the methods and a null model, $\hat{p} = \bar{Y}_{train}$.

	leukemia	brain cancer
PL-GCV	590.1	529.8
PL-PQL	585.6	529.5
SB	582.1	525.1
Geo	583.3	525.7
null	581.6	525.5

constant mean surface, \bar{Y}_{train} .

For real data, we do not know the true risk surface and do not report MSE as this is not appropriate for binary data. We can no longer calculate KL divergence by integrating with respect to the true distribution of the data, so we consider the log predictive density (LPD), $h(\mathbf{y}^*|\mathbf{y})$, on test data using a point estimate for the risk surface. To put the LPD on a more familiar scale, we sum across all the test observations in all 10 held-out sets and multiply by two, giving us a deviance measure, $D = -2 \sum_{m=1}^M (y_m^* \log \hat{p}_m + (1 - y_m^*) \log(1 - \hat{p}_m))$. While we are not in the situation of nested models with the associated testing theory, the difference in the deviances between the models gives some idea about how substantively different the predictions of the models are.

6.3 Results

The spectral basis, geoadditive model, and null models perform similarly, while the penalized likelihood methods appear to be overfitting, as they have higher deviances (Table 3) and estimate more variable spatial surfaces (not shown). Based on guidelines for interpreting log Bayes factors (Kass and Raftery 1995), which lie on the same scale, the higher deviances suggest some evidence against the penalized likelihood methods in favor of the SB, Geo and null models, but little evidence for choosing amongst the latter. The apparent overfitting of the penalized likelihood methods is consistent with the results of our simulation study.

With regard to substantive applied conclusions, based on the similarity between the deviances of the best fitting spatial models (SB and Geo) and the non-spatial null model, we cannot reject the null hypothesis that the risk is constant spatially. Even if one were to interpret the surfaces from the spectral basis model, there are not peaks in risk around the petrochemical complexes (Fig. 3). The increasing risk from north to south suggests there may be more risk near the southern-most complex, but without evidence that the risk is associated with the complex. The lack of higher risk near the complexes is not surprising, because the small number of individuals residing there gives us little power to detect changes in risk there. Note that this is a preliminary analysis that does not take account of covariates and is

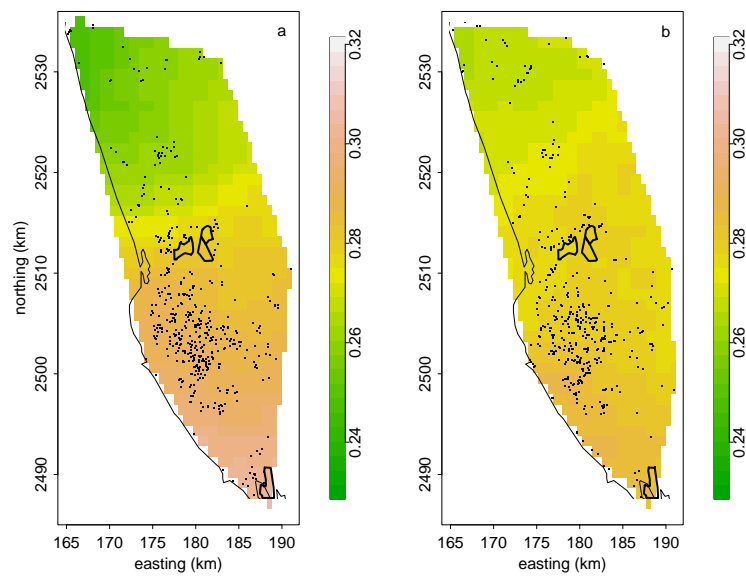


Figure 3. Posterior mean spatial surfaces (probability of being a case) based on the SB model for (a) leukemia and (b) brain cancer. Locations of observations are indicated by points, boundaries of petrochemical complexes by thick lines, and the coastline by the thin line.

intended solely as an illustration.

7 Discussion

Our simulations suggest that the spectral basis model is the best approach of those considered for fitting spatial logistic regression models. It provides a good compromise between quality of fit and computational speed, allowing the user to fit a model in a couple hours, or less time for a basic estimate of the spatial surface. A disadvantage is the coding effort required, but we provide template code in the electronic supplement and have released an R library, `spectralGP`. If the spectral basis model is too slow or too difficult to implement, or shows poor mixing for a particular dataset, the penalized likelihood methods are alternatives but are prone to overfitting. If computational speed is a concern, one may wish to use one of the penalized likelihood methods for data exploration and then the spectral basis method to confirm a small number of models. One could investigate the possibility of overfitting in the penalized likelihood models by comparing different smoothing parameters manually using cross-validation.

The methods assessed here are readily generalizable to other non-normal data; we have performed simulations with Poisson-distributed data and found that the results are similar to those here, with the spectral basis approach outperforming the other methods. As with binary data, the spectral basis approach does an excellent job of trading off between sensitivity and specificity, fitting somewhat better than the other methods on the simulation with a true signal, while avoiding the overfitting that occurs for the other methods on a null simulation.

The spectral basis model contains an implicit model complexity parameter, the range parameter, which combined with the multiresolution nature of the basis and the natural penalty on complexity implicit in the fully Bayesian approach (Denison et al. 2002, p.20) may help explain the superior performance of the spectral basis model. The multiresolution spectral basis model has basis functions at different frequencies, and the penalties on the coefficients (through the prior variances) are of different magnitude for the different frequencies. By estimating the range parameter, in addition to a variance parameter for the basis coefficients, the model adaptively changes the relative penalties at different frequencies. When the range parameter is large, the spectral density of the Matérn spatial correlation function produces very small prior variances for the high-frequency coefficients, essentially zeroing out these coefficients. This has the flavor of L_1 penalization, which Grandvalet (1998) has shown to be related to adaptive penalization. This adaptive penalization may help explain why the SB model does not overfit to the degree that other approaches do. The natural Bayesian complexity penalty favors large values of this parameter and smoother functions when that is consistent with the data. Zhang (2004) reports that only the ratio of the variance and range parameters can be estimated consistently, but we note that in the spectral basis model, the parameters have relatively low posterior correlation (0.24 in one example), suggesting that both parameters are needed in the model. In contrast, the PQL version of the penal-

ized likelihood model and its Bayesian implementation have only a single penalty/variance parameter; smoothing is accomplished by a penalty (the prior in the Bayesian implementation) on the magnitude of the coefficients, and the same penalty applies to all the coefficients, whose basis functions lie at the same level of resolution. The penalties on the basis coefficients in smoothing spline models (which is the form of the GCV penalized likelihood model) change with the basis frequency, but the relative penalties for different frequencies are fixed in advanced rather than adapting to the data (Brumback and Rice 1998).

All of the methods allow for the inclusion of additional covariates in a linear ($\mathbf{x}_i^T \boldsymbol{\beta}$ in (1)) or nonparametric fashion (substituting $\sum_p h_p(\mathbf{x}_i)$ for $\mathbf{x}_i^T \boldsymbol{\beta}$). The spectral basis and geoadditive representations of the spatial surface could also be included as modules in more complicated hierarchical models. These might be spatial-temporal models, models for multiple outcomes, or models that incorporate deterministic components. The success of the spectral basis model suggests its promise for use in representing spatial effects in more complicated models.

Our simulations and analysis of the Taiwan data ignore key aspects of spatial case-control data. First, the spatial logistic regression model does not analyze time to disease onset; spatial survival models such as that of Li and Ryan (2002) are one approach to this. Second, we assume individuals have fixed locations, while in reality individuals move over time, affecting their exposure. While a non-spatial model based on accurate exposure estimates is clearly a better approach than spatial logistic regression, there are reasons a spatial model may be preferred in certain circumstances. First, exposure estimates are usually very uncertain and may be unobtainable. The error introduced by assigning individuals to a fixed location may be of less concern than problems associated with an exposure estimate. Second, even when the spatial structure is not of primary interest, incorporating a spatial term in a model can be important to control for unmeasured covariates that may vary spatially. Furthermore, one may be interested in investigating spatial patterns in health outcomes in an exploratory hypothesis-generating fashion. Ideally, once a spatial pattern of risk is detected, more detailed investigation of potential risk factors and careful exposure estimation will be done.

Spatial models for binary outcomes have low statistical power, which plagues all of the methods, as can be seen in the lengths of the confidence and credible intervals. This difficulty arises from fitting a fully flexible bivariate surface with binary observations, which contain much less information than continuous or count observations. This is of particular concern for epidemiological data, for which both baseline risks and relative risks from exposure to disease-causing agents are often small. For cohort data, thousands of observations are necessary even to estimate simple surfaces with a single peak, such as the simulated dataset here, while more complicated surfaces, such as risks associated with roadways, would require either many more observations or very large relative risks from exposure. Even using case-control data with thousands of observations, the methods have relatively little power with realistic relative risks. When the risk is tied to a single point source, one might increase power by explicitly including distance to the source in the analysis (Morris and Wakefield 2000), such as by modelling a parametric risk function based on

distance to the source (Diggle 1990; Lawson 1993) or basing a hypothesis test on distance.

The low power for modelling the bivariate surface also makes it difficult to consider interactions between space and other covariates. In the Taiwan study, researchers are interested in gene by environment interactions. For a small number of genotypes, a simple approach would be to fit a separate spatial surface for each type, but this is unrealistic unless one has a large sample size and a small number of surfaces to fit. We have little power even without splitting the dataset, particularly given the small number of individuals residing near the petrochemical complexes.

Because of the low power, we have assessed the methods only on simple surfaces. The relative success of the methods may change for more complicated surfaces. With realistic binary epidemiological data, one is unlikely to be able to detect such surfaces, but in other applications, this may be more realistic.

8 Appendix: Representing functions in the spectral domain

The details in this appendix draw on Dudgeon and Mersereau (1984), Borgman, Taheri, and Hagan (1984), and Wikle (2002). The spectral basis approach represents a function, $g(\cdot)$, on a grid, $s^\#$, as a linear combination of orthogonal spectral basis functions, $g_{s^\#} = \mathbf{Z}\mathbf{u}$. The basis functions represented in the basis matrix, \mathbf{Z} , capture behavior at different frequencies, with the most important basis functions for function estimation being the low-frequency basis functions. The first step in representing the function is to choose the grid size, M_d , in each dimension, $d = 1, \dots, D$, to be a power of two. The M_d frequencies in the d th dimension are then $\omega^d \in \{0, 1, \dots, \frac{M_d}{2}, -\frac{M_d}{2} + 1, \dots, -1\}$, where the superscript represents the dimension. There is a complex exponential basis function for each distinct vector of frequencies, $(\omega_{m_1}^1, \dots, \omega_{m_D}^D)$, $m_d \in \{0, \dots, M_d - 1\}$, each with a complex-valued basis coefficient, u_{m_1, \dots, m_D} .

First we show how to construct a random, mean zero, Gaussian process in one dimension with domain $(0, 1)$ from the M spectral coefficients, $u_m = a_m + b_m i$, $m = 0, \dots, M - 1$, and complex exponential basis functions, $z_m(s_j) = \exp(2\pi i \omega_m s_j)$, whose real and imaginary components have frequency ω_m . To approximate real-valued processes, $u_0, \dots, u_{M/2}$ are jointly independent, u_0 and $u_{M/2}$ are real-valued ($b_0 = b_{M/2} = 0$), and the remaining coefficients are determined, $u_{M/2+1} = \bar{u}_{M/2-1}, \dots, u_{M-1} = \bar{u}_1$, where the overbar is the complex conjugate operation. This determinism causes the imaginary components of the basis functions to cancel, leaving a real-valued process,

$$\begin{aligned} g(s_j) &= \sum_{m=0}^{M-1} z_m(s_j) u_m = \sum_{m=0}^{\frac{M}{2}} \exp(2\pi i \omega_m s_j) (a_m + b_m i) + \sum_{m=\frac{M}{2}+1}^{M-1} \exp(2\pi i \omega_m s_j) (a_{M-m} - b_{M-m} i) \\ &= 2 \left(a_0 + \sum_{m=1}^{\frac{M}{2}-1} (a_m \cos(2\pi \omega_m s_j) - b_m \sin(2\pi \omega_m s_j)) + a_{M/2} \cos(2\pi \omega_{\frac{M}{2}} s_j) \right). \end{aligned}$$

Hence for a grid of M values, we approximate the process as a linear combination of M spectral basis functions corresponding to M real-valued sinusoidal basis functions, including the constant function ($\omega_0 = 0$). To approxi-

mate mean zero Gaussian processes with a particular stationary covariance function, the coefficients have Gaussian prior distributions with mean zero, while the spectral density for the covariance function, $f_\theta(\cdot)$, e.g., (6), determines the prior variance of the coefficients: $\mathbf{V}(u_m) = f_\theta(\omega_m) \Rightarrow \{\mathbf{V}(a_0) = f_\theta(\omega_0); \mathbf{V}(a_{M/2}) = f_\theta(\omega_{M/2}); \mathbf{V}(a_m) = \mathbf{V}(b_m) = \frac{1}{2}f_\theta(\omega_m), \text{ o.w.}\}$, with the coefficients a priori independent. The spectral basis represents periodic functions ($g(0) = g(2\pi)$), so the correlation function of the process on $(\pi, 2\pi)$ is the mirror image of the correlation function on $(0, \pi)$ with $\text{Cor}(g(0), g(2\pi)) = 1$. We avoid artifacts from this periodicity by mapping the interval $(0, 2\pi)$ to $(0, 2)$ and not using the process values on $(1, 2)$, thereby mapping the original domain of the observations to $(0, 1)$. Note that the use of $\pi\rho$ rather than ρ in (6) allows us to interpret ρ on the $(0, 1)$ rather than $(0, \pi)$ scale. The modelled surface is a piecewise constant surface on an equally-spaced grid of size $M/2 + 1$. This setup ensures that the correlation structure of the approximating process is close to the correlation structure of a GP with the desired stationary correlation function.

The setup is similar in two dimensions, with a matrix of coefficients, $((u_{m_1, m_2}))$, $m_d \in \{0, \dots, M_d - 1\}$, and corresponding frequency pairs, $(\omega_{m_1}^1, \omega_{m_2}^2)$. As seen in Table 4, many coefficients are again deterministically given by other coefficients to ensure that the process is a linear combination of real-valued sinusoidal basis functions of varying frequencies and orientations in \Re^2 . The real and imaginary components of each coefficient, $u_{m_1, m_2} = a_{m_1, m_2} + b_{m_1, m_2}i$, are again independent with $\mathbf{V}(a_{m_1, m_2}) = \mathbf{V}(b_{m_1, m_2}) = \frac{1}{2}f_\theta(\omega_{m_1}^1, \omega_{m_2}^2)$ and for $(m_1, m_2) \in \{(0, 0), (\frac{M_1}{2}, 0), (0, \frac{M_2}{2}), (\frac{M_1}{2}, \frac{M_2}{2})\}$, $b_{m_1, m_2} = 0$ and $\mathbf{V}(a_{m_1, m_2}) = f_\theta(\omega_{m_1}^1, \omega_{m_2}^2)$. Analogous to the one-dimensional case, we estimate a process on $(0, 1)^D$. To do so, we map the periodic domain $(0, 2\pi)^D$ to $(0, 2)^D$ and then map the observation domain onto the $(0, 1)^D$ portion (maintaining the scale ratio in the different dimensions, unless desired otherwise), ignoring the process values outside this region. Note that if the original domain is far from square, we unnecessarily estimate the process in large areas of no interest, resulting in some loss of computational efficiency.

In performing MCMC with two-dimensional processes for the situations described in this paper, we have found that sampling blocks of coefficients whose corresponding frequencies have similar magnitudes works well. We use smaller blocks for the low-frequency coefficients, thereby allowing these critical coefficients to move more quickly. The high-frequency coefficients have little effect on the function and are proposed in large blocks. The first block is the scalar, $u_{0,0}$, corresponding to the frequency pair, $(\omega_0^1, \omega_0^2) = (0, 0)$. The next block is the coefficients whose largest magnitude frequencies are at most one, i.e., u_{m_1, m_2} s.t. $\max\{|\omega_{m_1}^1|, |\omega_{m_2}^2|\} \leq 1$, but excluding the previous block, giving the block $\{u_{0,1}, u_{1,0}, u_{1,1}, u_{M_1-1,1}\}$. Recall that there are additional coefficients whose largest magnitude frequencies are at most one, e.g., u_{M_1-1, M_2-1} , but these are complex conjugates of the sampled coefficients. The next block is the coefficients whose largest magnitude frequencies are at most three, i.e., u_{m_1, m_2} s.t. $\max\{|\omega_{m_1}^1|, |\omega_{m_2}^2|\} \leq 3$, but excluding the previous block elements. The remaining blocks are selected in similar fashion, with the q th block containing the coefficients whose largest magnitude frequencies are at most $2^{q-1} - 1$. The real and imaginary components

Table 4. Visual display of the spectral coefficients for a two-dimensional process. The frequencies in each dimension are indicated by the row and column labels, with $h_d = \frac{M_d}{2}$ for $d = 1, 2$. The * operation indicates that one takes the matrix or vector, flips it in both the horizontal and vertical directions (just the horizontal or vertical in the case of a vector) and then takes the complex conjugates of the elements.

	0	1	...	h_2	$-h_2 + 1$...	-1
0	$u_{0,0}$	$u_{0,\cdot}$			u_{0,h_2}	$u_{0,\cdot}^*$	
1	$u_{\cdot,0}$	u_A			u_B^*		
⋮							
h_1							
$-h_1+1$	$u_{\cdot,0}^*$	u_B			u_A^*		
⋮							
-1							

of the coefficients in each block are proposed jointly, Metropolis-style, from a multivariate normal distribution with independent elements centered on the current values. Since the coefficients have widely-varying scales, we take the proposal variance for each coefficient to be the product of a tuneable multiplier (one for each block) and the prior variance of the coefficient, which puts the proposal on the proper scale.

References

- Albert, J. H. and Chib, S. (1993), "Bayesian analysis of binary and polychotomous response data," *Journal of the American Statistical Association*, 88, 669–679.
- Banerjee, S., Carlin, B., and Gelfand, A. (2004), *Hierarchical modeling and analysis for spatial data*: Chapman & Hall.
- Best, N., Arnold, R., Thomas, A., Waller, L., and Conlon, E. (1999), "Bayesian models for spatially correlated disease and exposure data," in *Bayesian Statistics 6*, eds. J. Bernardo, J. Berger, A. Dawid, and A. Smith, Oxford, U.K.: Oxford University Press, pp. 131–156.
- Best, N., Ickstadt, K., and Wolpert, R. L. (2000), "Spatial Poisson regression for health and exposure data measured at disparate resolutions," *Journal of the American Statistical Association*, 95, 1076–1088.
- Booth, J. G. and Hobert, J. P. (1999), "Maximizing generalized linear mixed model likelihoods with an automated Monte Carlo EM algorithm," *Journal of the Royal Statistical Society, Series B*, 61, 265–285.
- Borgman, L., Taheri, M., and Hagan, R. (1984), "Three-dimensional, frequency-domain simulations of geological variables," in *Geostatistics for Natural Resources Characterization, Part 1*, ed. e. a. Verly, G., D. Reidel Publishing Company, pp. 517–541.
- Breslow, N. (2003), "Whither PQL?" Technical Report 192, Department of Biostatistics, University of Washington.
- Breslow, N. E. and Clayton, D. G. (1993), "Approximate inference in generalized linear mixed models," *J. Am. Stat. Assoc.*, 88, 9–25.
- Brumback, B. A. and Rice, J. A. (1998), "Smoothing spline models for the analysis of nested and crossed samples of curves (C/R: p976-994)," *Journal of the American Statistical Association*, 93, 961–976.
- Carlin, B. P. and Louis, T. A. (2000), *Bayes and Empirical Bayes Methods for Data Analysis*: Chapman & Hall Ltd.
- Carroll, R., Ruppert, D., and Stefanski, L. (1995), *Measurement error in nonlinear models*, Boca Raton, Florida: Chapman & Hall

- Christensen, O. (2004), "Monte Carlo maximum likelihood in model-based geostatistics," *Journal of Computational and Graphical Statistics*, 13, 702–718.
- Christensen, O., Møller, J., and Waagepetersen, R. (2000), "Analysis of spatial data using generalized linear mixed models and Langevin-type Markov chain Monte Carlo," Technical Report R-002009, Department of Mathematics, Aalborg University.
- Christensen, O., Roberts, G., and Sköld, M. (2005), "Robust MCMC methods for spatial GLMMs," *JCGS*, in press.
- Christensen, O. F. and Waagepetersen, R. (2002), "Bayesian prediction of spatial count data using generalized linear mixed models," *Biometrics*, 58, 280–286.
- Cowles, M. K. and Carlin, B. P. (1996), "Markov chain Monte Carlo convergence diagnostics: A comparative review," *Journal of the American Statistical Association*, 91, 883–904.
- Cressie, N. (1993), *Statistics for Spatial Data* (Revised ed.): Wiley-Interscience.
- Denison, D. G., Holmes, C. C., Mallick, B. K., and Smith, A. F. M. (2002), *Bayesian Methods for Nonlinear Classification and Regression*, New York: Wiley.
- Diggle, P. J. (1990), "A point process modelling approach to raised incidence of a rare phenomenon in the vicinity of a prespecified point," *Journal of the Royal Statistical Society, Series A, General*, 153, 349–362.
- Diggle, P. J., Tawn, J. A., and Moyeed, R. A. (1998), "Model-based geostatistics," *Applied Statistics*, 47, 299–326.
- Dudgeon, D. and Mersereau, R. (1984), *Multidimensional Digital Signal Processing*, Englewood Cliffs, New Jersey: Prentice Hall.
- Elliott, P., Wakefield, J., Best, N., and Briggs, D. (2000), "Spatial epidemiology: methods and applications," in *Spatial epidemiology: methods and applications*, eds. P. Elliott, J. Wakefield, N. Best, and D. Briggs, Oxford University Press, pp. 3–14.
- Fahrmeir, L. and Lang, S. (2001), "Bayesian Inference for Generalized Additive Mixed Models Based on Markov Random Field Priors," *Journal of the Royal Statistical Society C*, 50, 201–220.
- Gamerman, D. (1997), "Sampling from the posterior distribution in generalized linear mixed models," *Statistics and Computing*, 7, 57–68.
- Gibbons, R. D. and Hedeker, D. (1997), "Random effects probit and logistic regression models for three-level data," *Biometrics*, 53, 1527–1537.

- Grandvalet, Y. (1998), "Least absolute shrinkage is equivalent to quadratic penalization," in *ICANN'98, Perspectives in Neural Computing*, Springer, pp. 201–206.
- Green, P. (1995), "Reversible jump Markov chain Monte Carlo computation and Bayesian model determination," *Biometrika*, 82, 711–732.
- Greenland, S. (1992), "Divergent biases in ecologic and individual-level studies," *Statistics in Medicine*, 11, 1209–1223.
- Hastie, T. J. and Tibshirani, R. J. (1990), *Generalized Additive Models*, London: Chapman & Hall Ltd.
- Hedeker, D. and Gibbons, R. D. (1994), "A random-effects ordinal regression model for multilevel analysis," *Biometrics*, 50, 933–944.
- Hobert, J. and Wand, M. (2000), "Automatic generalized nonparametric regression via maximum likelihood," Technical report, Department of Biostatistics, Harvard School of Public Health.
- Holmes, C. and Mallick, B. (2003), "Generalized nonlinear modeling with multivariate free-knot regression splines," *Journal of the American Statistical Association*, 98, 352–368.
- Kamman, E. and Wand, M. (2003), "Geoadditive models," *Applied Statistics*, 52, 1–18.
- Kass, R. and Raftery, A. (1995), "Bayes factors," *J. Am. Stat. Assoc.*, 90, 773–795.
- Lawson, A. B. (1993), "On the analysis of mortality events associated with a prespecified fixed point," *Journal of the Royal Statistical Society, Series A, General*, 156, 363–377.
- Lee, H. (2004), *Bayesian nonparametrics via neural networks*: SIAM.
- Lenk, P. J. (1999), "Bayesian Inference for Semiparametric Regression Using a Fourier Representation," *Journal of the Royal Statistical Society, Series B: Statistical Methodology*, 61, 863–879.
- Li, Y. and Ryan, L. (2002), "Modeling spatial survival data using semi-parametric frailty models," *Biometrics*, 58, 287–297.
- McCulloch, C. E. (1994), "Maximum likelihood variance components estimation for binary data," *Journal of the American Statistical Association*, 89, 330–335.
- (1997), "Maximum likelihood algorithms for generalized linear mixed models," *Journal of the American Statistical Association*, 92, 162–170.

- McCulloch, C. E. and Searle, S. R. (2001), *Generalized, linear, and mixed models*: John Wiley & Sons.
- Morris, S. and Wakefield, J. (2000), “Assessment of disease risk in relation to a pre-specified source,” in *Spatial epidemiology: methods and applications*, eds. P. Elliott, J. Wakefield, N. Best, and D. Briggs, Oxford University Press, pp. 153–184.
- Neal, R. (1993), “Probabilistic Inference Using Markov Chain Monte Carlo Methods,” Technical Report CRG-TR-93-1, Department of Computer Science, University of Toronto.
- (1996), *Bayesian Learning for Neural Networks*, New York: Springer.
- Ngo, L. and Wand, M. (2004), “Smoothing with mixed model software,” *Journal of Statistical Software*, 9.
- O’Connell, M. and Wolfinger, R. (1997), “Spatial regression models, response surfaces, and process optimization,” *Journal of Computational and Graphical Statistics*, 6, 224–241.
- Paciorek, C. (2003), *Nonstationary Gaussian Processes for Regression and Spatial Modelling*, unpublished Ph.D. dissertation, Carnegie Mellon University, Department of Statistics.
- Pan, B., Hong, Y., Chang, G., Wang, M., Cinkotai, F., and Ko, Y. (1994), “Excess cancer mortality among children and adolescents in residential districts polluted by petrochemical manufacturing plants in Taiwan,” *Journal of Toxicology and Environmental Health*, 43, 117–129.
- Rasmussen, C. E. and Ghahramani, Z. (2002), “Infinite mixtures of Gaussian process experts,” in *Advances in Neural Information Processing Systems 14*, eds. T. G. Dietterich, S. Becker, and Z. Ghahramani, Cambridge, MA: MIT Press.
- Richardson, S. (1992), “Statistical methods for geographic correlation studies,” in *Geographical and environmental epidemiology: methods for small-area studies*, eds. P. Elliott, J. Cuzick, D. English, and R. Stern, Oxford University Press, pp. 181–204.
- Ruppert, D., Wand, M., and Carroll, R. (2003), *Semiparametric regression*: Cambridge University Press.
- Shumway, R. and Stoffer, D. (2000), *Time Series Analysis and its Applications*, New York: Springer-Verlag.
- Wager, C. G., Coull, B. A., and Lange, N. (2004), “Modelling spatial intensity for replicated inhomogeneous point patterns in brain imaging,” *Journal of the Royal Statistical Society, Series B*, 66, 429–446.
- Wahba, G., Wang, Y., Gu, C., Klein, R., and Klein, B. (1995), “Smoothing spline ANOVA for exponential families, with application to the Wisconsin Epidemiological Study of Diabetic Retinopathy,” *The Annals of Statistics*, 23, 1865–1895.

- Waller, L. A., Carlin, B. P., Xia, H., and Gelfand, A. E. (1997), “Hierarchical spatio-temporal mapping of disease rates,” *Journal of the American Statistical Association*, 92, 607–617.
- Wikle, C. (2002), “Spatial modeling of count data: A case study in modelling breeding bird survey data on large spatial domains,” in *Spatial Cluster Modelling*, eds. A. Lawson and D. Denison, Chapman & Hall, pp. 199–209.
- Wolfinger, R. and O’Connell, M. (1993), “Generalized linear mixed models: A pseudo-likelihood approach,” *Journal of Statistical Computation and Simulation*, 48, 233–243.
- Wood, S., Jiang, W., and Tanner, M. (2002), “Bayesian mixture of splines for spatially adaptive nonparametric regression,” *Biometrika*, 89, 513–528.
- Wood, S. N. (2000), “Modelling and smoothing parameter estimation with multiple quadratic penalties,” *Journal of the Royal Statistical Society, Series B*, 62(2), 413–428.
- (2003), “Thin plate regression splines,” *Journal of the Royal Statistical Society, Series B*, 65(1), 95–114.
- (2004), “Stable and efficient multiple smoothing parameter estimation for generalized additive models,” *J. Am. Stat. Assoc.*, 99, 673–686.
- Zhang, H. (2004), “Inconsistent estimation and asymptotically equal interpolation in model-based geostatistics,” *J. Am. Stat. Assoc.*, 99, 250–261.
- Zhao, Y. and Wand, M. (2005), “Spatial statistics using general design Bayesian generalized linear mixed models: some applications,” *in submission*.

